



HAL
open science

Benchmarking of techniques used to assess the freeze damage in potatoes

Piyush Kumar Jha, Kévin Vidot, Epameinondas Xanthakis, Xavier Falourd, Joran Fontaine, Vanessa Jury, Alain E Le-Bail

► **To cite this version:**

Piyush Kumar Jha, Kévin Vidot, Epameinondas Xanthakis, Xavier Falourd, Joran Fontaine, et al.. Benchmarking of techniques used to assess the freeze damage in potatoes. *Journal of Food Engineering*, 2019, 262, pp.60-74. 10.1016/j.jfoodeng.2019.05.008 . hal-02539349

HAL Id: hal-02539349

<https://hal.science/hal-02539349v1>

Submitted on 25 Oct 2021

HAL is a multi-disciplinary open access archive for the deposit and dissemination of scientific research documents, whether they are published or not. The documents may come from teaching and research institutions in France or abroad, or from public or private research centers.

L'archive ouverte pluridisciplinaire **HAL**, est destinée au dépôt et à la diffusion de documents scientifiques de niveau recherche, publiés ou non, émanant des établissements d'enseignement et de recherche français ou étrangers, des laboratoires publics ou privés.



Distributed under a Creative Commons Attribution - NonCommercial 4.0 International License

1 **Benchmarking of techniques used to assess the freeze damage in potatoes**

2 **Piyush Kumar Jha**^{a, b, c}, **Kevin Vidot**^{c, d}, **Epameinondas Xanthakis**^e, **Xavier Falourd**^{c, d},
3 **Joran Fontaine**^{a, b, c}, **Vanessa Jury**^{a, b, c}, **Alain Le-Bail**^{a, b, c}

4 ^a ONIRIS, CS 82225, 44322 Nantes cedex 3, France

5 ^b UMR GEPEA CNRS 6144 - ONIRIS, 44322 Nantes cedex 3, France

6 ^c SFR IBSM 4204, 44316 Nantes, France

7 ^d UR 1268 Biopolymères Interactions Assemblages, INRA, 44316 Nantes, France

8 ^e RISE Research Institutes of Sweden – Agrifood and Bioscience, Gothenburg 41276, Sweden

9

10

11 *Corresponding authors:* Alain Le-Bail (alain.lebail@oniris-nantes.fr)

12

13 **Abstract**

14 In this study, benchmarking of methods used for assessing freeze damage in potatoes was
15 carried out. Initially, the samples were frozen by subjecting them to three different
16 temperatures (i.e. at $-18\text{ }^{\circ}\text{C}$, $-30\text{ }^{\circ}\text{C}$, and at $-74\text{ }^{\circ}\text{C}$). Then, different analytical techniques
17 comprising of focused methods (i.e. cryo-SEM, confocal laser scanning microscopy-CLSM)
18 and global methods (i.e. texture analysis, low field nuclear magnetic resonance (NMR),
19 exudate loss and colour change) were used to assess the impact of the freezing treatment from
20 the different point of view addressed by each method. As a result, each of these methods were
21 able to distinguish significantly fresh samples from the frozen-thawed samples. Focused
22 methods like cryo-SEM and CLSM methods could differentiate the impact of all three
23 different protocols. Meanwhile, texture analysis (including conventional method and novel
24 method based on a touchless laser puff firmness tester), NMR and exudate loss could only
25 determine the quality difference between $-18\text{ }^{\circ}\text{C}$ and $-74\text{ }^{\circ}\text{C}$ freezing conditions. Colour
26 analysis was found as an inappropriate parameter for comparing the three freezing protocols.
27 Among all analytical techniques, cryo-SEM provides the most authentic information about the
28 product as the analysis is performed in frozen state, while for other techniques the product is
29 thawed prior to analysis.

30 **1. Introduction**

31 Freezing is a preservation technique that has been used for ages for increasing the shelf life of
32 food products. Compared to other long-term preservation methods, freezing technique causes

33 less deterioration to nutrients and sensory properties in fruits and vegetables (Barbosa-
34 Cánovas, Altunakar & Mejía-Lorío (2005). However, it can cause some irreversible damages
35 such as texture loss, colour change, etc. Three main phenomena may describe freeze damage;
36 the primary mechanical effect caused by the transition of water into ice, the biochemical
37 effect caused by cryo-concentration and the secondary mechanical effect eventually caused by
38 ice contraction after freezing (Reid, 1997; Shi, Datta, & Mukherjee, 1999, 1998; Shi, Datta, &
39 Throop, 1998). The extent of freeze damage caused to the food products on thawing is greatly
40 linked to the size and location of the ice crystals, which in turn is related to the applied
41 freezing rate (Chevalier, Le Bail, & Ghoul, 2000). Freeze damage can also be linked to the
42 cryo-concentration effect; the aqueous solution present in the cells is exposed to a progressive
43 concentration in solute caused by ice formation. The remaining aqueous phase which tends to
44 become more and more concentrated can cause denaturation of the proteins and other
45 organized biopolymers (i.e. cellulose based systems for fruits and vegetables), which in turn
46 degrade their mechanical properties and by the way the overall texture of the tissue (Gao &
47 Critser, 2000; Lovelock, 1957; Reid, 1997). The mechanisms of freeze damage associated
48 with cryo-concentration effect have been thoroughly discussed in a review article from Gao &
49 Critser (2000). Rapid freezing (high freezing rate) favours the genesis of fine ice crystals
50 distributed uniformly within the product, thus reducing the dislocation of water from intra to
51 the extra cellular spaces, resulting in higher water holding capacity upon thawing. In addition,
52 the time of exposure to the highly concentrated aqueous solution caused by cryo-
53 concentration is being reduced during rapid freezing, resulting to a lesser extend of the
54 biochemical degradations (Delgado & Sun, 2001; Fennema, 1966; Orłowska, Havet, & Le-
55 Bail, 2009; Sadot, Curet, Rouaud, Le-bail, & Havet, 2017; Shi, Datta, & Mukherjee, 1998;
56 Singh & Heldman, 2009). The result is reduced cell destruction and better quality attributes.
57 However, two main disadvantages lie behind rapid freezing rates : (i) rapid freezing process
58 requires a higher amount of energy, hence increases the consumed energy and the overall
59 operating costs and (ii) the use of extremely high freezing rates such as cryogenic freezing,
60 may lead to crack development in the samples and yield unexpectedly poor quality of the final
61 product (secondary mechanical effect quoted above) (Shi, Datta, & Mukherjee, 1999, 1998;
62 Shi, Datta, & Throop, 1998). On the contrary, at a slow freezing rate, intracellular water move
63 to the extracellular domains (from the inside of the cell) and thus can result in greater ice
64 crystal size (in the extracellular spaces) and also in a higher cell dehydration (Gao & Critser,
65 2000; Mazur, 1984). Besides, slow freezing rate will also result in a prolonged exposition of
66 the tissue to the concentrated solution occurred from the cryo-concentration effect (Gao &

67 Critser, 2000; Mazur, 1977, 1984). In fact, the formation of larger ice crystals along with
68 volume shrinkage and long-term exposure to high solute concentrations would cause a higher
69 destruction of cellular structure (high risk of punctured cell membrane/cell wall, collapsed cell
70 structure and cell separation) (Chassagne-Berces et al., 2009; Chassagne-berces, Fonseca,
71 Citeau, & Marin, 2010; Gao & Critser, 2000; Mazur, 1984). As an outcome, the leakage of
72 the fluid from the cell will be higher and a product having a water-soaked appearance and
73 mushy texture will be obtained. The last important parameter that may be responsible for
74 quality losses of frozen foods is the storage conditions; time-temperature parameters, as well
75 as temperature fluctuations, are also responsible for the quality loss.

76 The assessment of the quality of a frozen food product is obtained via analytical methods used
77 to quantify the freeze damage. Broadly, these methods can be categorized as global methods
78 and focused methods. The global methods provide quality information at a macro/meso level.
79 In other terms, the quality information obtained using such methods is the average value from
80 a whole sample or at least from a substantial piece of sample (several grams or several cm³).
81 The global methods comprise of texture analysis, exudate loss measurement, solute
82 diffusivity, impedancemetry, colour analysis, etc. While the focused methods provide quality
83 information at a micro level (cell level or even at a lower scale such as ice crystal or water
84 molecule scale). For instance, information about ice crystals size, cellular structure intactness,
85 etc. can be obtained by using focused methods. Microstructures evaluation methods such as
86 Scanning electron microscopy (SEM) (includes conventional SEM, environmental SEM
87 (ESEM), and cryo-SEM), confocal laser scanning microscopy (CLSM), X-rays tomography,
88 etc. fall under focused method. Low field nuclear magnetic resonance relaxometry (NMR) is
89 at the same time a global and focused method as it embraces a sample of *circa* 1 cm³ scale
90 and provides info at the level of water molecules (Jha et al., 2018).

91 In the literature, numerous benchmarking studies are available related to freezing effects on
92 the quality parameters of the fruits and vegetables. However, no studies are available in the
93 literature that benchmarks the techniques used to assess the freeze damage in fruits and
94 vegetables.

95 This work was framed under the following objectives

- 96 i. To introduce new freeze damage assessment methods and check their efficiency in
97 quantifying the freeze damage.

98 ii. To benchmark the freeze damage methods (both conventional and novel) used for
99 assessing the freeze damage in plant-based products with the intention to facilitate the
100 researchers and industries to choose the appropriate method to assess the freeze damage.

101 The ultimate objective of this study is to provide a decision table which will allow to
102 categorize the analytical techniques based on sensitivity, efficiency, accuracy, cost of
103 operation, and ease of operation.

104 **2. Materials and methods**

105 **2.1. Product properties**

106 Potatoes (*Solanum tuberosum* L. cv. Innovator) were the food matrix chosen for this
107 benchmarking study. McCain Foods (Harnes, France) kindly supplied us potato batch having
108 uniform size and maturity. Two batches of potato were used for this test. The first batch of
109 potato was used for NMR tests. In order to reduce the variability, for each freezing condition,
110 samples intended for NMR test were taken from the same potato. Potatoes from the second
111 batch were used for time-temperature history study and freeze damage assessment tests. The
112 average moisture content of both batches was $75.70 \pm 1.40\%$ (wet basis) (Note: the values of
113 moisture content are presented here as mean \pm standard deviation. Similarly, the values for
114 other parameters in the entire manuscript are expressed as mean \pm standard deviation).

115 **2.2. Sample preparations**

116 The sample size used to study the effect of conventional freezing processes on the quality
117 parameters depended on the freeze damage assessment methods. For instance, to study the
118 effect of freezing rates on freezing characteristics, texture, colour and drip loss, cuboids of
119 potato ($1.3 \times 1.3 \times 1 \text{ cm}^3$ – length \times height \times width; weight $1.95 \pm 0.5 \text{ g}$) were used. The
120 potatoes were cut in cuboid shape using a dicer (Ibili Manage, Inc. Spain). The potato samples
121 used for NMR relaxometry and cryo-SEM analysis were cylindrical in shape ($\emptyset = 8 \text{ mm}$ and
122 $H = 10 \text{ mm}$). For confocal laser scanning microscopy (CLSM) analysis, cylindrical potato
123 samples ($\emptyset = 8 \text{ mm}$ and $H = 5 \text{ mm}$) were chosen. The samples were then immediately
124 transferred into the freezer and were cooled from the ambient temperature to the desired
125 temperature.

126 It is worth mentioning that during this study, one of our aims was to analyze the samples in its
127 original state without causing any alterations to them, thus we had to vary sample size for
128 potato according to the freeze damage assessment methods. For instance, NMR tube has an

129 internal diameter of 1 cm and hence required sample having a diameter < 1 cm. Also, another
130 requirement of NMR test is to have the NMR tube covered minimum up to 1 cm in height.
131 The cylindrical sample with a diameter of 8 mm and height of 1cm perfectly matched both the
132 requirements. For cryo-SEM, sample size similar as NMR facilitated easy cutting of sample in
133 the frozen state and allowed the selection of the analyzed sample from nearly the same
134 location for each condition. For CLSM, small sample size helped the proper and fast staining
135 of the sample and facilitated the selection of the analyzed sample from the same location of
136 each matrix.

137 **2.3. Freezing apparatus and freezing conditions**

138 Freezing of potatoes (unblanched) was performed at $-18\text{ }^{\circ}\text{C}$ in a cold room, at $-30\text{ }^{\circ}\text{C}$ and
139 0.5 m/s air velocity in an industrial batch freezer (MATAL, France), and at $-74\text{ }^{\circ}\text{C}$ in an
140 ultra-low temperature freezer (TSE240V, Thermo Scientific, Marietta, Georgia, USA). The
141 three conditions will be referred to as slow freezing (SF), intermediate freezing (IF) and fast
142 freezing (FF) in further sections of the manuscript. Once frozen, the samples were packed in
143 the zip-lock and stored at $-40 \pm 2\text{ }^{\circ}\text{C}$ (\approx for 2-3 days) until quality evaluation tests were
144 performed. The time-temperature profile during the freezing tests was studied by inserting a
145 K-type thermocouple at a geometric centre of the product. The (thermocouple) was calibrated
146 against a reference platinum probe (Comptoir Lyon Allemand – Lyon-France). During
147 measurements the temperature of the sample was recorded every 2 s with a data logger with
148 an accuracy of $\pm 0.1\text{ }^{\circ}\text{C}$. For comparison purposes, temperature profiles from the initial
149 temperature $18\text{ }^{\circ}\text{C}$ to $-18\text{ }^{\circ}\text{C}$ were considered. The characteristic freezing time and overall
150 freezing time were determined using time-temperature data. The characteristic freezing time
151 was the measure of local freezing rate and it was defined as the time during which the
152 temperature at a particular point changed from the initial freezing point to a temperature at
153 which 80% of the water (at that point) was converted into ice. The temperature range
154 considered for the characteristic freezing time estimation was from -1 to $-7\text{ }^{\circ}\text{C}$, similar
155 temperature range was used by Li & Sun (2002) for the determination of characteristic
156 freezing time during ultrasound assisted freezing of potatoes. The overall freezing time was
157 the time required to lower the temperature of the geometrical centre of the product from the
158 ambient temperature ($18\text{ }^{\circ}\text{C}$) in the present study) to a given temperature ($-18\text{ }^{\circ}\text{C}$). Samples
159 for quality analysis were frozen using the same procedure but without optical fibre inserted.
160 Each experiment was performed at a minimum of individual triplicates.

161 **2.4. Thawing protocol**

162 The frozen potato samples were thawed at room temperature (20 ± 1 °C) for 2 h in a zip-lock
163 bag (“static air thawing” method) before performing colour, drip loss, texture and solute
164 diffusion measurements. For NMR analysis the samples were thawed at 4 °C for 4 h in the
165 NMR tube.

166 **2.5. Colour analysis**

167 The colour of the potatoes was measured using a portable and handheld chroma meter CR-
168 400 (Konica Minolta, Inc. Japan). Using this equipment, the L^* , a^* , b^* values for samples from
169 each condition were obtained with high accuracy. The maximum value for L^* is 100
170 (represents a perfectly white surface or a perfectly reflecting diffuser) and its minimum value
171 is 0 (represents perfectly black surface). The positive and negative a^* corresponds to red and
172 green colour. Similarly, positive and negative b^* represents yellow and blue colour,
173 respectively. A single value for the colour difference was achieved by calculating the overall
174 colour difference (ΔE) value; it takes into account the differences between L^* , a^* , b^* of the
175 specimen (e.g. frozen-thawed sample) and reference (fresh sample), and it was calculated by
176 using Eq. (1) (Anon, 2018). The frozen samples were thawed before the colour measurements.
177 At least eight measurements were recorded for each freezing protocol.

$$\Delta E = \sqrt{\Delta L^{*2} + \Delta a^{*2} + \Delta b^{*2}} \quad (1)$$

178

179 **2.6. Drip loss measurement**

180 The drip loss required great care in terms of manipulation. The mass differences that are being
181 determined are usually small and it can be advantageous to use paper tissue to collect all the
182 drip released by a sample. This requires the weight of the bag containing the sample, the
183 initial mass of the tissue paper and all the final masses. There is also a risk of moisture
184 condensation on the sample during frozen storage (if unpacked) or during the thawing process
185 or even sample handling after thawing if their temperature is lower than the dew point
186 temperature. The drip loss unit is very often given as g drip per g of sample. In most existing
187 studies, drip losses are expressed as free drip; this means that drip the collected from the
188 sample due to gravity forces and possible capillary interactions with the tissue paper. In some
189 studies, the samples are compressed under selected stress (Jahncke, Baker, & Regenstein,
190 1992) or after centrifugation for selected g values under given times (Penny, 1975). In our

191 study, the drip loss was determined based on the weight difference between frozen sample
192 (W_1), and thawed sample (W_2). The drip loss (%) was calculated using Eq. (2). At least 9
193 samples were analyzed for each freezing condition.

$$\text{Drip Loss (\%)} = \frac{W_1 - W_2}{W_1} \times 100 \quad (2)$$

194

195 **2.7. Texture analysis**

196 Texture analysis of food is often carried out using the TPA protocol (Texture Profile
197 Analysis) proposed by Bourne (Bourne, 1968). Quite often, simple compression tests are used
198 for frozen food aiming at determining the Young's Modulus (small deformation, typically
199 10% strain) and eventually the failure strain or stress. In our study, the frozen potato samples
200 were thawed and compressed in a texture analyser (AMETEK, Lloyd Instruments, France)
201 equipped with a 1000 N load cell and operating at a test speed of 50 mm/min beyond failure
202 point which was marked by a significant drop in the force reading (Figure 1). The
203 compression test was performed using a 50 mm compression plate. A similar procedure was
204 used by Khan & Vincent (1993, 1996) for determining the failure stress, Young's Modulus,
205 and failure strain of potato. Based on our preliminary trials and the results from Khan &
206 Vincent (1993) and Alvarez, et al. (2002), compression of the sample to 50% strain was found
207 more than sufficient to cause the failure of our sample (Figure 1). The maximum force exerted
208 during the compression test was recorded as the firmness/hardness (N) of the samples (Figure
209 1). Moreover, the stress vs. strain curves during compression tests were examined and
210 Young's modulus (E) (the slope of the loading curve at the point of its highest gradient) was
211 also acquired (Chassagne-Berces et al., 2009). All measurements were performed at $21 \pm 2^\circ\text{C}$.
212 At least 12 samples were analyzed for each freezing condition.

213 **2.7.1. Laser-puff firmness tester**

214 A touchless laser-puff firmness tester which was designed and constructed in our lab (GEPEA
215 lab, ONIRIS) was used for non-destructive measuring of the texture of fresh and frozen-
216 thawed potatoes (Figure 2). The firmness tester consists of the following components: a mean
217 to generate impulsive jet of air; a nozzle (having a diameter of 0.004 m) to direct the air onto
218 the surface of the specimen under investigation; a deformation measurement unit containing a
219 laser source to generate coherent source of light directed on the surface of the object impacted
220 by the air jet, a detector of the light which is reflected from the specimen surface, and an

221 analyzer to estimate the amount of deformation sustained by the product surface; a control
222 panel to change the pressure value and an appropriate software (developed in our lab) to
223 execute the test. Based on the preliminary trials, for measuring the firmness of frozen-thawed
224 potatoes, the air nozzle was located at 10 mm from the food surface and an air pressure of $5 \times$
225 10^5 Pa and air jet exposure time of 100 ms were found most appropriate. The estimated
226 pressure exerted onto the food surface was in the range of 3.32×10^5 Pa assuming a surface of
227 1.256×10^{-5} m² impacted by the air jet. Prussia, Astleford, Hewlett, & Hung (1994) used
228 impact pressure of 3.10×10^5 Pa (45 psia) in order to determine the firmness of potato.
229 Similar to the authors, Hung, McWatters, & Prussia (1998) who used the same exposure time
230 to determine the firmness of peaches.

231 The sample was placed on the sample platform below the air delivery nozzle and the position
232 of sample was adjusted using a positioner in order to ensure (i) the air jet and the laser hits the
233 same point on the sample and (ii) the distance between end of the nozzle and the sample
234 surface is same for all trials. Subsequently, by using the software air jet was directed on the
235 sample and the deformation was measured. The software yielded deformation results in volts
236 (Figure 3). The maximum deformation can be referred to as the difference between the
237 highest initial value and lowest value recorded by the deformation unit during the test. The
238 conversion of volts to mm (millimeter) based unit was made by multiplying with a conversion
239 factor (in the present case, volt value was multiplied by 2 to obtain final value in mm). The
240 final deformation value was an average of sixteen measurements.

241 **2.8. Microstructure examination**

242 **2.8.1. Cryo-SEM analysis**

243 Cryo-SEM analysis is a very specific technique which requires very careful and proper
244 sample preparation. A thin specimen of slab shape was cut from a given location of the frozen
245 food using a sharp scalpel. In our case, the central section of the frozen potato samples was
246 selected for collecting the sample. Also, in the case of structured tissue, given shape must be
247 provided to the sample to identify a given orientation; for example, in the case of a muscle,
248 the longer section of sample is usually longitudinal to the fibers in order to be able to do cut
249 view either parallel or perpendicular to the fibers. In the case of a vegetal tissue has no major
250 orientation so special care was taken mainly for the location, shape and size of the sample. It
251 was fixed into the groove notched in a copper sample holder (10 mm diam. 10 mm height)
252 using an OCT (optimal cutting temperature) compound (Tissue-Tek, Sakura, Finetek, USA).

253 An important technical issue lies in preventing any thawing of sample when the sample is
254 contacted onto the sample order. To overcome this difficulty, the following protocol was
255 used. All manipulations were done in a cold box filled with CO₂ sticks (-78.5 °C) in order to
256 condition the sample which was kept in this ambience. The sample holder was refreshed down
257 to around 0 °C by contacting a CO₂ stick. Then a small amount of OCT was installed in the
258 groove of the sample holder. Then, at the same time, the sample holder was contacted onto a
259 CO₂ stick meanwhile the frozen sample was contacted to the OCT located in the groove.
260 Within less than a few seconds, the sample was fixed onto the sample holder thanks to the
261 freezing of the OCT. The very high thermal diffusivity of the copper material (sample holder)
262 compared to the frozen sample ensures that the sample will not undergo any thawing when the
263 sample is contacted to the sample holder. The sample was left for 2 min in a box filled with
264 dry CO₂ to harden the OCT compound. After that, the sample was loaded onto a precooled
265 copper specimen stub (in liquid N₂) and was quickly transferred in the cryo-preparation
266 chamber of the cryo-SEM (LS10, ZEISS EVO, Germany) maintained under vacuum at - 80
267 °C, where it was cryo-fractured using a precooled sharp knife mounted inside the chamber.
268 The fractured sample was etched in the preparation chamber for about 5 to 10 min to expose
269 the subsurface information in order to allow a partial sublimation of the ice crystals. The
270 etching time required adjustment depending on the size of the sample, the pressure level and
271 the type of tissue. The sample was finally coated with a thin conducting layer of gold (5 nm)
272 in the cryo-preparation chamber and then was transferred to the cold stage in the cryo-SEM
273 (maintained at - 80 °C) where microstructural observation was performed. The fractured
274 surfaces of potatoes were examined with an accelerating voltage of 11 kV. An illustration of
275 the sample preparation steps is presented in Figure 4. It is worth mentioning that all the
276 samples prepared for cryo-SEM analysis after the different freezing conditions acquired from
277 the same potato.

278 **2.8.2. Confocal laser scanning microscopy (CLSM)**

279 The confocal laser scanning microscopy was also used for potatoes samples. Figure 5
280 provides a brief description of the protocol followed to prepare potatoes for the CLSM
281 observations. The CLSM was performed using an Eclipse Ti inverted microscope (Nikon Ti
282 A1, Japan). For each freezing condition, independent experiments were performed in
283 triplicates.

284 It is worth noticing that the acridine orange (used for this study) is well known to be a

285 metachromic dye, especially for staining DNA and RNA. Such dye is able to give
286 fluorescence with emissions wavelength depended on its interaction with chemical functions,
287 charge or geometry of a compound. The acridine orange was chosen here as a dye able to
288 stain simultaneously the different cell layers of the fruits as it has been widely applied for
289 fluorescent staining of plant tissue with a high fluorescence emission. The maximum emission
290 wavelength of this dye is 500-530 nm and excitation occurs at about 488 nm.

291 **2.9. NMR relaxometry**

292 For all the freezing protocols, NMR tests were performed for samples in frozen state (at -20
293 $^{\circ}\text{C}$) and frozen-thawed state (at 4 $^{\circ}\text{C}$). Initially, the frozen samples were placed in the NMR
294 tube ($\varnothing = 10$ mm) precooled to -20 $^{\circ}\text{C}$. Then the tube was quickly placed in the
295 spectrometer (maintained at -20 $^{\circ}\text{C}$) and left for 10 min to ensure that the samples were at
296 -20 $^{\circ}\text{C}$ at the beginning of NMR test at a negative temperature. Upon completion of NMR
297 tests in frozen condition, the same samples were thawed (at 4 $^{\circ}\text{C}$ for 4 h) and then NMR tests
298 on frozen-thawed samples (at 4 $^{\circ}\text{C}$) were carried out. In order to compare the damage caused
299 by different freezing procedures, the NMR measurements of fresh samples were performed at
300 4 $^{\circ}\text{C}$ and were compared with results obtained for frozen-thawed samples obtained under
301 various freezing protocols. The Minispec mq20 spectrometer (Bruker) at 0.47 T (20 MHz
302 proton resonance frequency) equipped with a thermostated (± 0.1 $^{\circ}\text{C}$) ^1H probe was used for
303 NMR analysis. Triplicates were performed for each freezing condition of potato.

304 In the present study, T_2 (transverse) relaxation time of protons and their respective population
305 in the product were evaluated. The T_2 distributions were determined using a
306 Carr–Purcell–Meiboom–Gill (CPMG) sequence. For the NMR test at frozen and frozen-
307 thawed state, the 180° pulse separation was 0.04 and 0.1 ms, 2000 and 10000 even echoes
308 were collected, and the 1024 and 256 scans were acquired with a recycle delay of 1 and 5 s
309 resulting in a total acquisition time of about 20 and 40 min respectively.

310 An inverse Laplace transformation (ILT) was applied to convert the relaxation signal into a
311 continuous distribution of T_2 relaxation components. For this purpose, a numerical
312 optimization method was used by including non-negativity constraints and L1 regularization
313 and by applying a convex optimization solver primal–dual interior method for convex
314 objectives (PDCO).

315 **2.10. Statistical analysis**

316 One-way ANOVA (analysis of variance) was used to determine any significant difference (in
317 terms of freezing and quality characteristics) among the freezing conditions. Duncan's
318 multiple range test was performed to determine differences between the means ($p < 0.05$).

319 **3. Results and discussion**

320 **3.1. Effect of different freezing rates on temperature history**

321 The representative temperature histories of potatoes frozen under the different freezing
322 conditions are presented in Figure 6. The SF process yielded freezing curves having three
323 stages i.e. the supercooling, nucleation, and phase change. Meanwhile, intermediate freezing
324 (IF) exhibited only two stages (i.e. nucleation and phase change stages) and fast freezing (FF)
325 showed only one stage (i.e. phase change state) in Figure 6. SF condition gave a degree of
326 supercooling of 0.15 ± 0.07 °C, while no supercooling curve was observed for the other two
327 freezing conditions. Similar freezing curves lacking obvious supercooling at higher freezing
328 rates (at -80 °C and liquid nitrogen immersion freezing) were also obtained by Cao et al.
329 (2018) during freezing of blueberries. It was inferred by them that at a faster freezing rate the
330 supercooled state might be unstable or lack persistence. The initial freezing point for SF and
331 IF condition was recorded as -0.3 ± 0.14 and -0.73 ± 0.06 °C (Table 1). It seems that a
332 slight depression in freezing point happened upon increasing the freezing rate. For FF
333 condition, it was hard to detect the initial freezing point due to a rapid decline in the
334 temperature during the freezing process. However, more replications could be helpful to be
335 conducted prior to the confirmation of this outcome. Recently, Cao et al. (2018) also reported
336 slight decrease (but not significant) in the initial freezing temperature of blueberries when the
337 freezing rate was increased from 0.023 °C/s (at -20 °C) to 0.049 °C/s (at -40 °C) or 0.11 °C/s
338 (at -80 °C) or 0.76 °C/s (liquid nitrogen immersion freezing). The initial freezing point of
339 blueberries at 0.023 , 0.049 , 0.11 , and 0.76 °C/s rates were recorded as -2.67 ± 0.32 °C,
340 -3.23 ± 0.12 °C, -3.53 ± 0.35 °C and -3.36 ± 0.60 °C respectively (Cao et al., 2018).
341 Among other freezing parameters being studied, the characteristic freezing time was found to
342 be the shortest for FF condition (8.52 ± 1.53 min), followed by IF and SF condition
343 (17.18 ± 0.79 min and 29.12 ± 3.94 min respectively) (Table 1). The time spent in this zone
344 is very crucial as it determines the quality of the final product. From the perspective of higher
345 quality preservation, a shorter width of this zone is desired. Similar to characteristic freezing
346 time, the overall freezing time and the overall freezing rate also exhibited a similar trend.

347 **3.2. Texture analysis**

348 **3.2.1. Conventional method**

349 The confined compression test was the conventional method used to determine the texture of
350 potatoes. The hardness and Young's modulus values of fresh and thawed sample (from
351 different freezing conditions) are shown in Table 2. The values of fresh samples were
352 significantly different ($p < 0.05$) compared with those of the frozen-thawed samples. FF
353 process caused less decay in hardness value ($\approx 50\%$) than IF process ($\approx 62\%$) or SF process
354 ($\approx 74\%$). However, significant differences in hardness values were observed only between SF
355 and FF samples. Young's modulus values exhibit a similar tendency as hardness values in
356 Table 2.

357 Khan & Vincent (1996) reported that compressive stiffness of potato less degraded when
358 freezing was performed at a higher freezing rate ($10\text{ }^{\circ}\text{C}/\text{min}$) compared to slow freezing rate
359 ($1\text{ }^{\circ}\text{C}/\text{min}$). According to Mazur (1984) and Chassagne-Berces, Fonseca, et al. (2010), lower
360 dehydration associated with small ice crystals induced less breakage of cell walls, and hence,
361 better texture preservation was achieved at higher freezing rates when compared to the slow
362 freezing rate. The high freezing rates also decrease the collapse of cell walls and generate less
363 intercellular spaces, and hence result in better texture preservation (Chassagne-Berces et al.,
364 2009). Besides, Phinney, Frelka, Wickramasinghe, & Heldman (2017) reported that the
365 extent of texture loss of potato depends on the freezing time. It was found that the hardness of
366 thawed potato reached a maximum value when the freezing time decreased dramatically up to
367 1000 s. Further, increase in freezing time beyond 1000 s to around 5000 s did not cause any
368 further texture loss in their case. Van Buggenhout et al. (2006) evaluated the effect of three
369 different freezing conditions i.e. slow freezing (freezing time (f_t) = 300 min), rapid freezing (f_t
370 = 40 min)) and cryogenic freezing (f_t = 10 min)) on the hardness retention of thawed carrots.
371 They reported that rapid and cryogenic freezing condition had a higher hardness retention
372 than the slow freezing condition.

373 **3.2.2. Laser-Puff firmness tester**

374 Laser-Puff firmness tester allows rapid and non-destructive texture analysis of the food
375 products (Hung et al., 1998; McGlone & Jordan, 2000; Prussia et al., 1994). An attempt was
376 made to use this method, to the best of our knowledge for the first time, for measuring the
377 texture of frozen-thawed fruits and vegetables. In this section, the results from laser-puff
378 firmness analysis of potato will be presented and discussed. The deformation curves and
379 deformation values obtained during laser-puff firmness test of fresh and frozen-thawed

380 potatoes (under different freezing rates) are shown in Figure 7. The fresh samples had
381 significantly ($p < 0.05$) lower deformation value than all frozen-thawed samples (Figure 7b).
382 As expected, SF samples suffered the highest deformation during the tests. The deformation
383 occurred at IF samples was less than SF samples, but greater than the FF samples. However,
384 the deformation values of IF samples were not significantly different ($p > 0.05$) from the
385 values of SF and FF samples. The FF sample showed lower deformation than the other
386 conditions, and those values were found to be significantly lower than SF, but not
387 significantly different from IF values. The obtained results (in terms of deformation) are
388 coherent with those obtained by the classical method (discussed above). In conclusion, this
389 method could distinguish fresh and frozen-thawed samples, but had limited capability to
390 differentiate the tested freezing conditions.

391 **3.3. NMR relaxometry**

392 NMR tests were performed for the samples in frozen (at $-20\text{ }^{\circ}\text{C}$) and frozen-thawed states (at
393 $4\text{ }^{\circ}\text{C}$) after being frozen under the different freezing conditions. Figure 8 shows the results
394 from NMR relaxometry of potato in a frozen state (at $-20\text{ }^{\circ}\text{C}$). The relaxation peaks, T_2^*
395 (including magnetic field inhomogeneities) and T_2 of frozen samples provide information
396 about the structure of the samples and about the unfrozen water at $-20\text{ }^{\circ}\text{C}$ (Figure 8). $T_{2\alpha}^*$ is
397 the relaxation peak of protons associated with the macromolecules. $T_{2\beta}^*$, $T_{2\gamma}$, and $T_{2\delta}$ are the
398 relaxation peaks associated with the protons of unfrozen water (Foucat & Lahaye, 2014;
399 Luyts et al., 2013). Results showed that the $T_{2\alpha}^*$ values (relaxation time and proton population)
400 for all freezing conditions were similar, which indicated that the different freezing protocols
401 didn't influence differently the systems at a macromolecular level (Figure 8a). Similarly, $T_{2\beta}^*$
402 values were not significantly different among the different freezing conditions (Figure 8a). If
403 we follow the hypothesis that the faster the freezing process is the less is the destruction it
404 imparts, the values of relaxation peak components of non-freezable water ($T_{2\gamma}$ and $T_{2\delta}$)
405 associated with the samples frozen quickly provide an evidence of better preservation of
406 structures. Only samples that were frozen slowly (at $-18\text{ }^{\circ}\text{C}$) showed different values for
407 these relaxation peak components (Figure 8a and b). It was observed that $T_{2\gamma}$ component
408 values (relaxation time and proton population) for IF and FF conditions were not significantly
409 different ($p > 0.05$) between each other, meanwhile, these values were significantly different
410 ($p < 0.05$) with that obtained for SF condition. The lowest value of $T_{2\gamma}$ time observed for slow
411 freezing (0.72 ms instead of around 0.80 ms for the other freezing conditions) can be

412 explained by a greater destruction followed by a diffusion of "solutes" inducing a relative
413 increase in viscosity (Lahaye, Falourd, Limami, & Foucat, 2015). The $T_{2\delta}$ component
414 relaxation times for all freezing conditions were not different from each other. But, the
415 $T_{2\delta}$ component proton population was significantly lower ($p < 0.05$) for SF compared to the
416 other conditions. This seemed to indicate the loss of fluid from the respective water
417 compartment due to greater damage occurred during SF process. No significant difference (p
418 > 0.05) (with respect to $T_{2\delta}$ component proton population) was observed among IF and FF
419 samples.

420 Figure 9 represents the T_2 peaks of fresh and frozen-thawed samples at 4 °C. With regard to
421 fresh samples, the distribution of T_2 relaxation peak has five components (T_{2a} , T_{2b} , T_{2c} , T_{2d} &
422 T_{2e}), whose values averages are in good agreement with the literature data (Rutledge, Rene,
423 Hills, & Foucat, 1994). Based on these data, an allocation of different components of T_2 have
424 been proposed: T_{2a} and T_{2b} are the relaxation peaks associated with the water present in the
425 cell walls and the vacuolar membrane. T_{2c} is the relaxation peak of water in starch grains. T_{2d}
426 and T_{2e} are the relaxation peaks of water in the non-starch vacuoles, the nucleus and the
427 cytoplasm (Rutledge et al., 1994). The measurement of the T_2 components values (relaxation
428 time and proton population) of the samples after thawing makes it possible to observe the
429 influence of different freezing protocols on the mobility of the water compared with the fresh
430 samples. It can be seen that the freezing-thawing process affects the resolution of the T_2
431 distribution peaks (Figure 9). For instance, the T_{2c} and T_{2d} components which were
432 distinctively visible in the fresh sample could no longer be differentiated in the frozen-thawed
433 sample. Apart from this, T_{2d} and T_{2e} times of fresh potato decreased upon freezing-thawing.

434 Among the different freezing conditions used in this study, only FF (at - 74 °C) preserved T_2
435 components distributions with good resolution over the entire time range studied. Four T_2
436 components were characterized for FF (against five for fresh samples), meanwhile, for IF and
437 SF conditions, three and two T_2 components could only be characterized. For all freezing
438 conditions, the mobility of water associated with non-starch vacuoles, nuclei and cytoplasm
439 (T_{2d} and T_{2e}) decreased. This reflects a reorganization of the fluids following a partial rupture
440 of the cellular structures (Lahaye et al., 2015) irrespective of the freezing speed. Compared to
441 fresh sample, the decrease in T_{2e} time was lower for FF process ($\approx 46\%$) and was followed by
442 SF ($\approx 53\%$) and IF ($\approx 54\%$) process. However, no significant difference among freezing
443 processes (in terms of T_{2e} time) was observed. T_{2e} component proton population data reveal

444 that FF and IF samples had similar values ($p > 0.05$) as the fresh sample, while it significantly
445 decreased ($p < 0.05$) in the case of SF samples. This decrease was followed by an increase in
446 proton population of the consecutive peak in the T_2 distribution curve for SF samples (Figure
447 9b), depicting the transfer of water between two compartments which might have probably
448 happened due to the breakdown of vacuolar membrane. However, no such trend was observed
449 for other freezing conditions (Figure 9c and d). The T_2 component values (relaxation time and
450 proton proportion) adjacent to the T_{2e} for SF samples was significantly different ($p < 0.05$)
451 from those of FF and IF conditions. The T_{2a} and T_{2b} components of FF samples had similar
452 relaxation times as the fresh samples, illustrating the overall better preservation of membranes
453 and walls (despite a reorganization at the level of populations). IF also fairly maintained the
454 T_{2b} component values and they were found to be similar to the fresh sample. Due to poor
455 resolution, it was difficult to extract T_{2a} component value for IF samples. T_{2a} and T_{2b}
456 component values for SF sample also could not be resolved due to the poor resolution of the
457 peak.

458 Cao et al. (2018) used T_2 time of water proton to differentiate fresh blueberries from frozen-
459 thawed blueberries. They found that the freezing-thawing process caused a reduction in T_2
460 time of vacuole, cell wall, cytoplasm and extracellular water compared to the fresh sample.
461 With respect to the proton population of different compartments, it was observed that freezing
462 and thawing did not cause any alteration in the proton population of different compartments
463 compared to a fresh samples. Moreover, they also used T_2 relaxation peak data to distinguish
464 different freezing conditions (i.e. freezing at -20 , -40 , -80 °C and freezing by immersing in
465 liquid nitrogen). It was reported that among all freezing conditions, -80 °C freezing
466 conditions better maintained T_2 time of vacuole ($p < 0.05$) depicting better protection to the
467 vacuole membrane. Unlike them, we did not observe any significant difference among the
468 freezing trials with respect to the relaxation times of thawed samples frozen by different
469 methods, however, we could observe a significant differences between FF, IF and SF
470 conditions with respect to the proton population of T_2 peaks. The proton population data
471 (associated with T_2 times) was used by Zhang et al. (2018) to study the effect of state/phase
472 transition on water mobility in frozen mango during 4-week storage.

473 **3.4. Drip loss**

474 Drip loss is one of the commonly and widely used methods to evaluate the freeze damage in
475 frozen products (especially in meat, fish, fruits and vegetable matrices). This method

476 estimates the freeze damage at a global level, or in other terms, provides an average value of
477 freeze damage of a product. In this section the impact of the studied freezing conditions on the
478 exudate loss from the product will be presented and discussed. Figure 10 shows the
479 dependence of drip loss on freezing rate. The results reveal that drip loss decreased slightly
480 when freezing rate was increased, however, significant difference was observed only between
481 samples that were frozen under FF and SF conditions. IF samples were not significantly
482 different ($p > 0.05$) compared to the samples of the other two freezing rates. The drip loss
483 results exhibited similar trends to those of T_{2e} component proton population from NMR that
484 showed that the application of $-18\text{ }^{\circ}\text{C}$ freezing protocol maintained less the intracellular
485 water content. This result may be attributed to a better preservation of the intracellular water
486 and to a lower damage of the pectocellulosic walls from the faster freezing rates. As a result,
487 this method was able to detect the differences between the selected freezing rates. The water
488 holding capacity of the frozen sample is linked to the size and location of ice crystals as well
489 as the thawing rate (Van Buggenhout, Messagie, et al., 2006). The formation of large ice
490 crystals in the cellular matrix can affect the water holding capacity of a cellular matrix in two
491 ways: (i) large ice crystals genesis during freezing can damage the cell membrane due to
492 mechanical effects, to cryo-concentration phenomena and shrinkage effects (particularly
493 during slow freezing rates) which in turn, will promote loss of mass during thawing
494 (Bevilacqua, Zaritzky, & Calvelo, 1979; Delgado & Sun, 2001; Sadot et al., 2017) and (ii)
495 higher drip loss may occur due to the formation of bigger ice crystals which correspond to
496 smaller specific surface area. This fact is associated with water re-absorption decrease during
497 thawing (Bevilacqua et al., 1979; Sadot et al., 2017). Charoenrein & Owcharoen (2016) and
498 Fuchigami, Hyakumoto, & Miyazaki (1995) observed decrease in exudate loss with
499 increasing freezing rates in frozen mangoes and carrots.

500 **3.5. Colour**

501 Freezing-thawing process significantly ($p < 0.05$) affected the colour parameters (L^* , a^* , and
502 b^* values) of the unblanched potatoes Figure 11. The L^* value (or lightness) and b^* value (or
503 yellowness) decreased, while the a^* value (redness) increased for potatoes after freezing-
504 thawing (Figure 11a, b and c). These results are in agreement with the previously reported
505 study on freezing-thawing of unblanched potatoes (Koch et al., 1996). The colour change
506 during the freezing-thawing process of unblanched potato has been attributed to the browning
507 reaction that generally happens due to enzymatic activity during thawing process (Cano,
508 1996; Koch et al., 1996). The freezing rates had little effect on the colour parameters of

509 potatoes. Interestingly, it was found that FF process increased the redness value of potatoes
510 significantly ($p < 0.05$) than compared to SF process. Chassagne-berces, Fonseca, et al.
511 (2010) reported that freezing at $-80\text{ }^{\circ}\text{C}$ increased the redness value of Golden Delicious apple
512 compared to the one frozen at $-20\text{ }^{\circ}\text{C}$. The redness value of IF samples was not significantly
513 different compared with those frozen under FF and SF conditions. No significant differences
514 for rest of the colour parameters (L^* value, b^* value and ΔE) were observed among the
515 freezing protocols.

516 **3.6. Microstructure analysis**

517 **3.6.1. Cryo-SEM analysis**

518 Scanning electron microscopy permits to obtain very high-quality images of a food matrix
519 microstructure. With respect to the frozen cellular matrices, micrographs acquired using SEM
520 (especially the cryo-SEM) provide important details about ice and cell morphology (shape of
521 the cell and the integrity of pectocellulosic walls). To the best of our knowledge, for the first
522 time, cryo-SEM was used to compare the changes occurring to the microstructure of potato at
523 different freezing rates. Figure 12 illustrates the SEM images of fresh and frozen potatoes.
524 The images of fresh and frozen potato were obtained using an environmental SEM (E-SEM)
525 and cryo-SEM, respectively. It can be seen in the figure that the fresh potato has polyhedral
526 shape cells with starch embedded in it. The microstructure morphology upon freezing
527 depended highly on the freezing rate being applied. The SF process not only created bigger
528 ice crystals in the cells but also caused the highest damage to the cellular structure. The cells
529 were highly distorted (deformed cells with broken and irregular cell wall structure) under SF
530 conditions. The IF process produced smaller ice crystals and maintained the cell wall integrity
531 better than the SF conditions. However, some cells lost their polyhedral shape and turned
532 almost into round shape when freezing was performed at IF conditions (cells pointed by the
533 orange arrow in Figure 12e and Figure 12f). The FF process yielded smallest ice crystals
534 compared to other freezing processes. Moreover, it can also be observed that the cellular
535 structure (in terms of cell shape i.e. polyhedral shape and cell wall integrity) was maintained
536 well. Similar to the authors, Bomben & King (1982), Chassagne-Berces et al. (2009) and
537 Chassagne-Berces, Fonseca, et al. (2010) cryo-SEM imaging could differentiate the apples
538 frozen by different freezing conditions based on microstructure. Moreover, they also observed
539 that slow freezing process (e.g. freezing at $-20\text{ }^{\circ}\text{C}$ or 0.4 K/min) altered the shape of the cell
540 more than the fast freezing processes (e.g. freezing at $-80\text{ }^{\circ}\text{C}$ or 450 K/min or by liquid
541 nitrogen immersion freezing). The calculations for ice crystals size were not made as it was

542 difficult to locate the boundary of the ice crystals. Moreover, the ice crystals had a 3D
543 structure and if the calculation were made, we could get only 2D information, this would have
544 led to an inaccurate estimation of the size of the ice crystals. Chassagne-Berces et al. (2009)
545 quantified the size of ice crystals formed at different freezing protocols (at $-20\text{ }^{\circ}\text{C}$, $-80\text{ }^{\circ}\text{C}$
546 and by immersion in liquid nitrogen) from the cryo-SEM images using gray level
547 granulometry based on mathematical morphology. They reported that the size of ice crystals
548 was between 10 and 30 μm after freezing at $-20\text{ }^{\circ}\text{C}$ and below 5 μm for faster freezing at
549 $-80\text{ }^{\circ}\text{C}$ and by immersion in liquid nitrogen conditions. Since we were not able to quantify
550 the size of ice crystals, a direct comparison with their results remained difficult.

551 **3.6.2. CLSM analysis**

552 CLSM images of fresh and frozen-thawed potatoes are presented in Figure 13. This method
553 provides information about the status of the cell such as the shape of cells and integrity of the
554 cell wall. Compared to the fresh sample, the cells were highly disorganised and distorted in
555 SF samples. The altered shape of the cells and damaged cell wall structures in the slowly
556 frozen sample can be observed in the CLSM images (Figure 13). The buckled and folded cell
557 wall structure in SF samples indicated a major dehydration related damage that generally
558 happens at lower freezing rates (Chassagne-Berces et al., 2009; Gao & Critser, 2000; Mazur,
559 1977, 1984). IF process affected the cell shape as cell walls were found slightly distorted,
560 while IF seemed to have fairly preserved the integrity of the cellular structure and avoid cell
561 wall rupture as observed by SF. Moreover, extracellular spaces that can be generated due to
562 the freezing-thawing process were observed in IF samples (Figure 13c), while it was missing
563 in FF samples (Figure 13d). It can be seen (Figure 13c and Figure 14c) that these gaps were
564 adjacent to the shrunk cells, which clearly indicates the dislocation of water from the inner of
565 the cell to the extracellular space. It was difficult to distinguish freezing-thawing induced gaps
566 between the cells in SF sample as the structure was completely destroyed. FF condition
567 helped to preserve the original shape and integrity of the cellular structure. The results from
568 CLSM (in terms of cell morphology) were coherent with the results from cryo-SEM.
569 Charoenrein & Owcharoen (2016) used CLSM to study the effect of freezing rates and freeze-
570 thaw cycles on the cellular structure of mangoes. Using this method, they were able to
571 observe the freezing-thawing related degradation of cellular structure. Moreover, based on
572 CLSM images, they were able to discriminate the different freezing protocols (i.e. freezing at
573 -80 , -40 and $-20\text{ }^{\circ}\text{C}$). For instance, CLSM micrographs depicted that cells observed after
574 fast freezing (at $-80\text{ }^{\circ}\text{C}$) and thawing suffered a minimal amount of degradation; the cells

575 were still round and similar to cells from fresh tissues. The IF frozen (at $-40\text{ }^{\circ}\text{C}$)-thawed
576 sample showed a slightly flat cellular structure, while the slow frozen (at $-20\text{ }^{\circ}\text{C}$)-thawed
577 mangoes exhibited larger changes. The cells of the slowly frozen samples lacked uniformity
578 and some intercellular spaces were also observed in slowly frozen tissues. Sirijariyawat,
579 Charoenrein, & Barrett (2012) used CLSM to study the change in cellular morphology in
580 mangoes upon freezing-thawing. They reported that freezing (at $-50\text{ }^{\circ}\text{C}$) followed by storage
581 (at $-20\text{ }^{\circ}\text{C}$ chest freezer for 14 days) and thawing (at $4\text{ }^{\circ}\text{C}$ for 2 h and kept at $25\text{ }^{\circ}\text{C}$ for 30
582 min prior to analysis) of mango samples transformed the well-defined circular to elliptical
583 regular cells of fresh sample to irregular shaped cells with disintegrated cell wall.

584 **4. Conclusions**

585 In this study, potato samples were frozen under different freezing regimes and their quality
586 were evaluated using different techniques. The slowly frozen ($-18\text{ }^{\circ}\text{C}$) potatoes exhibited
587 supercooling during freezing while no supercooling was noticed for other freezing conditions
588 (i.e. $-30\text{ }^{\circ}\text{C}$ - intermediate freezing process and $-74\text{ }^{\circ}\text{C}$ - fast freezing process). The initial
589 freezing point (initial freezing temperature) could be detected for slow freezing and
590 intermediate freezing conditions, while it was hard to detect the initial freezing point for the
591 fast freezing condition. The initial freezing point temperature data for slow freezing and
592 intermediate freezing conditions revealed that a depression in freezing point occurred when
593 freezing rate was increased. The slow freezing process resulted in coarser ice crystals and also
594 caused the highest damage to the cellular structure. The cells were highly distorted (deformed
595 cells with buckled and folded cell wall structure) when the slow freezing condition was used.
596 Intermediate freezing rate process led to relatively fine ice crystals compared to slow freezing
597 process. Although IF process led to greater cell wall structure integrity, however, it was not
598 able to preserve the cell shape. The fast freezing process not only promoted the formation of
599 very fine ice crystals but also preserved the morphology of the cells. The NMR analytical
600 parameters, texture and drip loss showed limitations to differentiate the different freezing
601 protocols. . None of the freezing protocols preserved the colour parameters of the fresh potato.

602 **Benchmarking of freeze damage assessment methods for vegetables on the basis of** 603 **efficiency, accuracy, cost-of operation, and ease of operation**

604 In this section, freeze damage assessment methods used during this study were evaluated
605 based on various benchmarking parameters and a decision table (dedicated to benchmarking
606 study) was proposed. Table 3 summarizes the results obtained within this study. Pros and cons

607 related to the different methods considered in this study for assessing the freeze damage in
608 potato were discussed.. These observations would provide useful information about the
609 analytical techniques that can be used to estimate freeze damage efficiently.

610 The focused freeze damage assessment technologies like CLSM, and global freeze damage
611 assessment techniques like texture analysis (also includes laser-puff texture analysis), low
612 field NMR relaxometry, and colour analysis tests used in this study was found to be relevant
613 methods to distinguish the fresh samples from frozen/thawed sample.

614 The acquired results suggest that cryo-SEM and CLSM are suitable for validating minor
615 quality changes among the different freezing protocols. Meanwhile, the global methods such
616 as texture, NMR, and drip loss can only reflect larger quality changes.

617 In order to compare freezing protocols, colour analysis was found to be an unsuitable
618 parameter.

619 Efficiency and accuracy wise, cryo-SEM and CLSM can be termed as best methods to
620 analyze the freezing injuries.

621 NMR, cryo-SEM and CLSM techniques are expensive techniques, whereas texture analysis,
622 drip loss measurements, colour analysis are cost-effective technologies. The analyses time for
623 NMR is long, while other methods take substantially less time.

624 From a global point of view, a debate could be opened on which is the most relevant
625 technique to assess freeze damage. Two key parameters can be tackled, (i) the size of the field
626 that is embraced by the technique and (ii) the representative size of the technique. For
627 example, NMR will tackle a sample of ca 1 cm and will provide information at the level of a
628 water molecule (2.75 Å). Cryo-SEM will look at field of ca 100 µm with information at
629 nanometer scale, even though in this case the freeze damage is observed at the scale of an ice
630 crystal (*circa* 10 µm). The ratio between the size of field and the representative size of
631 technique could be considered as a kind of “freeze damage assessment index” (FDA Index) to
632 assess the relevance of each technique. The higher the FDA index will be, the useful will be
633 (*a priori*) the technique. From such point of view NMR looks like the best candidate, even
634 though the interpretation and quantification of the freeze damage based on T_1 and T_2 values
635 are not very well documented in the literature and still remain quite subjective. The major
636 concerns relates to the size of the field. Observation of the freeze damage on a single cell can
637 be very informative and detailed, but ca a hundred of cell should be analyzed to obtain an

638 averaged information, which is out of reach for time reasons. Another aspect relies on the
639 possibility to repeat the analysis and on the time needed for a single measurement. CLSM and
640 Cryo-SEM bring informative images that can help to visualize the defaults and that can
641 support observations done with other techniques at a broader field like NMR, texture, drip
642 losses. The precision of the analytical method is one of the most important factors when choosing the
643 methods for freeze damage assessment. A method that imparts minimum error to the measured result
644 will help in better understanding of the impact of process conditions on the sample. Based on the error
645 calculations made for the quantitative methods (Table 3), the drip loss measurement seemed to be
646 more satisfactory , followed by colour analysis, hardness analysis, deformation analysis by the laser-
647 puff tester, NMR analysis and Young's Modulus analysis. Overall, the error imparted by the
648 analytical techniques were quite low in values.

649 The proper assessment of freeze damage remains a challenge and requires a mass of
650 experimental work before drawing any conclusion. However, this comparative study is maybe
651 the first one that proposes a benchmarking of so many different analytical techniques often
652 considered to assess the freeze damage.

653 **Acknowledgements:**

654 This work received financial support from the French National Research Agency (ANR) and
655 the Swedish Research Council FORMAS under the FREEZEWAVE project (SUSFOOD-
656 ERANET, FR: ANR-14-SUSF-0001, SE: 2014-1925). We would like to thank Anthony Ogé
657 (ONIRIS) for designing the laser-puff firmness tester. A special thanks to McCain food for
658 supplying potatoes required for the experimentation. The authors would also like to thank
659 Romain Mallet (Univ-Angers - SCIAM) for their assistance in cryo-SEM imaging
660 respectively.

661

- 663 Alvarez, M. D., Canet, W., & López, M. E. (2002). Influence of deformation rate and degree
664 of compression on textural parameters of potato and apple tissues in texture profile
665 analysis. *European Food Research and Technology*, 215, 13–20.
- 666 Anon (2018). <http://cobra.rdsor.ro/cursuri/cielab.pdf>. Retrieved on 3rd July 2018.
- 667 Barbosa-Cánovas, G. V., Altunakar, B., & Mejía-Lorío, D. J. (2005). Introduction to freezing.
668 *Freezing of fruits and vegetables: An agribusiness alternative for rural and semi-rural*
669 *areas* (Vol. 158, pp. 1-36). Rome: Food & Agriculture Organization.
- 670 Bevilacqua, A., Zaritzky, N. E., & Calvelo, A. (1979). Histological measurements of ice in
671 frozen beef. *Journal of Food Technology*, 14, 237–251.
- 672 Bomben, J. L., & King, C. J. (1982). Heat and mass transport in the freezing of apple tissue. *J.*
673 *Fd Technol.*, 17, 615–632.
- 674 Bourne, M. C. (1968). Texture Profile of Ripening Pears. *Journal of Food Science*, 33, 223–
675 226.
- 676 Cano, M. P. (1996). Vegetables. In L. E. Jeremiah (Ed.), *Freezing effects on food quality* (pp.
677 247–298). New York: Marcel Dekker, Inc.
- 678 Cao, X., Zhang, F., Zhao, D., Zhu, D., & Li, J. (2018). Effects of freezing conditions on
679 quality changes in blueberries. *Journal of the Science of Food and Agriculture*, 98, 4673–
680 4679.
- 681 Charoenrein, S., & Owcharoen, K. (2016). Effect of freezing rates and freeze-thaw cycles on
682 the texture, microstructure and pectic substances of mango. *International Food Research*
683 *Journal*, 23, 613–620.
- 684 Chassagne-berces, S., Fonseca, F., Citeau, M., & Marin, M. (2010). Freezing protocol effect
685 on quality properties of fruit tissue according to the fruit, the variety and the stage of
686 maturity. *LWT - Food Science and Technology*, 43, 1441–1449.
- 687 Chassagne-Berces, S., Poirier, C., Devaux, M. F., Fonseca, F., Lahaye, M., Pigorini, G.,
688 Girault, C., Marin, M., & Guillon, F. (2009). Changes in texture, cellular structure and
689 cell wall composition in apple tissue as a result of freezing. *Food Research International*,
690 42, 788–797.
- 691 Chevalier, D., Le Bail, a., & Ghou, M. (2000). Freezing and ice crystals formed in a
692 cylindrical food model: Part II. Comparison between freezing at atmospheric pressure
693 and pressure-shift freezing. *Journal of Food Engineering*, 46, 287–293.
- 694 Delgado, A. E., & Sun, D. W. (2001). Heat and mass transfer models for predicting freezing
695 processes – a review. *Journal of Food Engineering*, 47, 157–174.
- 696 Fennema, O. (1966). An over-all view of low temperature food preservation. *Cryobiology*,
697 3(3), 197–213.
- 698 Foucat, L., & Lahaye, M. (2014). Short communication A subzero ¹H NMR relaxation
699 investigation of water dynamics in tomato pericarp. *Food Chemistry Journal*, 158, 278–
700 282.
- 701 Fuchigami, M., Hyakumoto, N., & Miyazaki, K. (1995). Programmed Freezing Affects
702 Texture, Pectic Composition and Electron Microscopic Structures of Carrots. *Journal of*
703 *Food Science*, 60, 137–141.
- 704 Gao, D., & Critser, J. K. (2000). Mechanisms of Cryoinjury in Living Cells. *ILAR Journal*,
705 41, 187–196.
- 706 Hung, Y. C., McWatters, K. H., & Prussia, S. E. (1998). Peach Sorting Performance of
707 Anondestructive Laser Air-Puff Firmness Detector. *Applied Engineering in Agriculture*,
708 14, 513–516.
- 709 Jahncke, M., Baker, R. C., & Regenstein, J. M. (1992). Frozen storage of unwashed cod
710 (*Gadus morhua*) frame mince with and without kidney tissue. *Journal of Food Science*,

711 57, 575–580.

712 Jha, P. K., Xanthakis, E., Chevallier, S., Jury, V., & Le-Bail, A. (2018). Assessment of freeze
713 damage in fruits and vegetables. *Food Research International*. In press, accepted article.

714 Khan, A. A., & Vincent, J. F. V. (1993). Compressive Stiffness and Fracture Properties of
715 Apple and Potato Parenchyma. *Journal of Texture Studies*, 24, 423–435.

716 Khan, A. A., & Vincent, J. F. V. (1996). Mechanical damage induced by controlled freezing
717 in apple and potato. *Journal of Texture Studies*, 27, 143–157.

718 Koch, H., Seyderhelm, I., Wille, P., Kalichevsky, M. T., & Knorr, D. (1996). Pressure-shift
719 freezing and its influence on texture, colour, microstructure and rehydration behaviour of
720 potato cubes. *Nahrung*, 40, 125–131.

721 Lahaye, M., Falourd, X., Limami, A. M., & Foucat, L. (2015). Water mobility and
722 microstructure evolution in the germinating medicago truncatula seed studied by NMR
723 relaxometry. A revisited interpretation of multicomponent relaxation. *Journal of*
724 *Agricultural and Food Chemistry*, 63, 1698–1710.

725 Li, B., & Sun, D. W. (2002). Effect of power ultrasound on freezing rate during immersion
726 freezing of potatoes. *Journal of Food Engineering*, 55, 277–282.

727 Lovelock, J. E. (1957). The denaturation of lipid-protein complexes as a cause of damage by
728 freezing. *Proceedings of the Royal Society of London. Series B, Biological Sciences*, 147,
729 427–433.

730 Luyts, A., Wilderjans, E., Waterschoot, J., Haesendonck, I. Van, Brijs, K., Courtin, C. M.,
731 Hills, B., & Delcour, J. A. (2013). Low resolution 1H NMR assignment of proton
732 populations in pound cake and its polymeric ingredients. *Food Chemistry*, 139, 120–128.

733 Mazur, P. (1977). The role of intracellular freezing in the death of cells cooled at
734 supraoptimal rates. *Cryobiology*, 14, 251–272.

735 Mazur, P. (1984). Freezing of living cells: mechanisms and implications. *American Journal of*
736 *Physiology–Cell Physiology*, 247, C125–142.

737 McGlone, V. A., & Jordan, R. B. (2000). Kiwifruit and apricot firmness measurement by the
738 non-contact laser air-puff method. *Postharvest Biology and Technology*, 19, 47–54.

739 Orłowska, M., Havet, M., & Le-Bail, A. (2009). Controlled ice nucleation under high voltage
740 DC electrostatic field conditions. *Food Research International*, 42, 879–884.

741 Penny, I. F. (1975). Use of a centrifuging method to measure the drip of pork Longissimus
742 dorsi slices before and after freezing and thawing. *Journal of the Science of Food and*
743 *Agriculture*, 26, 1593–1602.

744 Phinney, D. M., Frelka, J. C., Wickramasinghe, A., & Heldman, D. R. (2017). Effect of
745 Freezing Rate and Microwave Thawing on Texture and Microstructural Properties of
746 Potato (*Solanum tuberosum*). *Journal of Food Science*, 82, 933–938.

747 Prussia, S. E., Astleford, J. J., Hewlett, B., & Hung, Y. C. (1994). 5,372,030. U.S. Patent and
748 Trademark Office.

749 Reid, D. S. (1997). Overview of physical/chemical aspects of freezing. In M. C. Erickson &
750 Y.-C. Hung (Eds.), *Quality in frozen food* (pp. 10–28). Dordrecht: Springer
751 Science+Business Media.

752 Rutledge, D. N., Rene, F., Hills, B. P., & Foucat, L. (1994). Magnetic resonance imaging
753 studies of the freeze-drying kinetics of potato. *Journal of Food Process Engineering*, 17,
754 325–352.

755 Sadot, M., Curet, S., Rouaud, O., Le-bail, A., & Havet, M. (2017). Numerical modelling of an
756 innovative microwave assisted freezing process. *International Journal of Refrigeration*,
757 80, 66–76.

758 Shi, X., Datta, A. K., & Mukherjee, Y. (1998). Thermal Stresses From Large Volumetric
759 Expansion During Freezing of Biomaterials. *Transactions of the ASME*, 120, 720–726.

760 Shi, X., Datta, A. K., & Mukherjee, Y. (1999). Thermal fracture in a biomaterial during rapid

761 freezing. *Journal of Thermal Stresses*, 22, 275–292.
762 Shi, X., Datta, A. K., & Throop, J. A. (1998). Mechanical Property Changes during Freezing
763 of a Biomaterial. *Transactions of the ASAE*, 41, 1407–1414.
764 Singh, R. P., & Heldman, D. R. (2009). Food Engineering. In S. L. Taylor (Ed.), *Introduction*
765 *to Food Engineering* (4th ed., pp. 501–541). San Diego: Academic Press publications.
766 Sirijariyawat, A., Charoenrein, S., & Barrett, D. M. (2012). Texture improvement of fresh and
767 frozen mangoes with pectin methylesterase and calcium infusion. *Journal of the Science*
768 *of Food and Agriculture*, 92, 2581–2586.
769 Van Buggenhout, S., Lille, M., Messagie, I., Von Loey, A., Autio, K., & Hendrickx, M.
770 (2006). Impact of pretreatment and freezing conditions on the microstructure of frozen
771 carrots: Quantification and relation to texture loss. *European Food Research and*
772 *Technology*, 222, 543–553.
773 Van Buggenhout, S., Messagie, I., Maes, V., Duvetter, T., Loey, A. Van, & Hendrickx, M.
774 (2006). Minimizing texture loss of frozen strawberries: effect of infusion with
775 pectinmethylesterase and calcium combined with different freezing conditions and effect
776 of subsequent storage / thawing conditions. *European Food Research and Technology*,
777 223, 395–404.
778 Zhang, Y., Zhao, J. H., Ding, Y., Xiao, H. W., Sablani, S. S., Nie, Y., Wu, S.-J., & Tang, X.
779 M. (2018). Changes in the vitamin C content of mango with water state and ice crystals
780 under state/phase transitions during frozen storage. *Journal of Food Engineering*, 222,
781 49–53.

782

783

784 **Captions for the Figures**

785

786 Figure 1: Load-strain curve providing detail about the firmness of the potato during the
787 compression tests.

788

789 Figure 2: Laser-puff firmness testing prototype.

790

791 Figure 3: A representative deformation curve obtained while performing the laser puff test.
792 Conversion of volts to mm: 1 V = 2 mm.

793

794 Figure 4: Illustration of sample preparation step prior to imaging in cryo-SEM.

795

796 Figure 5: Protocol followed for CLSM imaging of unblanched potato.

797

798 Figure 6: Representative freezing curves of potatoes under different freezing methods.

799

800 Figure 7: (a) Deformation curve obtained for fresh and frozen-thawed samples (conversion of
801 volts to mm: 1 V = 2 mm) and (b) deformation values (in mm) for fresh and frozen-thawed
802 potatoes (under different freezing rates) acquired using laser-puff firmness tester. SF (slow
803 freezing at $-18\text{ }^{\circ}\text{C}$), IF (intermediate freezing at $-30\text{ }^{\circ}\text{C}$) and FF (fast freezing at $-74\text{ }^{\circ}\text{C}$).

804

805 Figure 8: Distributions of relaxation peak components ((a) T_2^* and (b) T_2) at $-20\text{ }^{\circ}\text{C}$ of potato
806 samples frozen by various freezing protocols: slow freezing at $-18\text{ }^{\circ}\text{C}$ (red lines),
807 intermediate freezing at $-30\text{ }^{\circ}\text{C}$ (blue lines), and fast freezing at $-74\text{ }^{\circ}\text{C}$ (black lines). (The
808 x-axis correspond to the relaxation times expressed in ms (milliseconds)).

809 Figure 9: T_2 relaxation peak data of frozen-thawed potatoes at $4\text{ }^{\circ}\text{C}$: (a) fresh sample, (b) after
810 freezing at $-18\text{ }^{\circ}\text{C}$ (c) after freezing at $-30\text{ }^{\circ}\text{C}$ and (d) after freezing at $-74\text{ }^{\circ}\text{C}$.

811 Figure 10: Effect of different freezing conditions on the drip loss of potato.

812 Figure 11: Effect of freezing protocols on color parameters (a - L^* value or Lightness, b - a^*
813 value or Redness, c - b^* value or Yellowness and d - ΔE) of potato. Mean values of 9
814 repetitions are represented with confidence interval.

815

816 Figure 12: Microstructure of potato before and after freezing under the different freezing
817 protocols. (a, b) environmental SEM images of the fresh cell showing the cellular structure
818 and starch granules imbedded into it. Cryo-SEM after freezing at $-18\text{ }^{\circ}\text{C}$ -SF (c, d), at -30
819 $^{\circ}\text{C}$ -IF (e, f) and at $-74\text{ }^{\circ}\text{C}$ -FF (g, h), respectively. White colored arrows in images are
820 pointing the cells containing ice crystals. Red arrow showing the area where the breakdown of
821 cell structure happened. Orange arrows indicate the cells that might have transformed from
822 polyhedral to almost round shape. Other abbreviations in the picture are A: air space; S: starch
823 granule; W: cell wall structure.

824

825 Figure 13: Microstructure evaluation using CLSM: (a) fresh potato, (b) frozen-thawed after
826 freezing at $-18\text{ }^{\circ}\text{C}$ -SF, (c) at $-30\text{ }^{\circ}\text{C}$ -IF and (d) at $-74\text{ }^{\circ}\text{C}$ -FF. Other abbreviations in the
827 picture are S: starch granule, W: cell wall, S_p is probably the gap created when of cell moved
828 apart from each other as a consequence of freezing-thawing. The red arrows indicating the
829 deformed, distorted and shrunk cells. Orange arrows indicating loss of regularity of the cell

830 walls compared to fresh and FF samples. Yellow arrows showing the folded and buckled cell
831 wall structure formed due to SF process.
832

833 Figure 14: Microstructure evaluation using CLSM: (a) single cell of fresh potato, (b) single
834 potato cell (imaged in frozen state) after freezing at $-18\text{ }^{\circ}\text{C}$ (SF), (c) frozen-thawed potato
835 structure after frozen at $-30\text{ }^{\circ}\text{C}$ (IF) and (d) frozen-thawed potato structure after frozen at
836 $-74\text{ }^{\circ}\text{C}$ (FF) (d). S_p is probably the gap between the cells created due to freezing-thawing
837 process. Black arrow showing a part of broken cell wall. White arrow indicating discontinuity
838 in the cell wall structure. Red arrow evince the deformed cell with irregular cell wall structure
839 (orange arrows).

840

841

842

843

844

845

846

847

848

849

850 **Captions for Tables**

851 Table 1. Effects of different freezing protocols on the freezing properties of potatoes.

852 Table 2. Textural parameters measured for potatoes under different freezing conditions.

853 Table 3. Benchmarking study on freeze damage assessment methods.

854

855

856

857

858

859

860

861

862

863

864

865

866

867

868

869

870

871

872

873

874

875

876

877

878

879

880 Table 1. Effects of different freezing protocols on the freezing properties of potatoes.

Freezing condition	Initial freezing point (°C)	Characteristic freezing time (min)	Overall freezing time (min)	Overall freezing rate (°C/min)
– 18 °C (SF)	– 0.3 ± 0.14	29.12 ± 3.94	72.30 ± 0.14	0.48 ± 0.00
– 30 °C (IF)	– 0.73 ± 0.06	17.18 ± 0.79	26.31 ± 0.62	1.36 ± 0.05
– 74 °C (FF)	n.d.	8.52 ± 1.53	14.51 ± 1.49	2.51 ± 0.25

881

882

883 Table 2. Textural parameters measured for potatoes under different freezing conditions.

Parameters	Hardness (N)	Young's modulus (MPa)
Fresh	190 ± 19^a	5.46 ± 0.44^a
SF (at $-18\text{ }^\circ\text{C}$)	47 ± 11^c	1.37 ± 0.33^c
IF (at $-30\text{ }^\circ\text{C}$)	$68 \pm 16^{b,c}$	$2.09 \pm 0.41^{b,c}$
FF (at $-74\text{ }^\circ\text{C}$)	90 ± 8^b	2.60 ± 0.45^b

884

885

886

887

888

889

890

891

892

893

894

895

896

897

898

899

900

901

902

903

904

905

906 Table 3. Benchmarking study on freeze damage assessment methods.

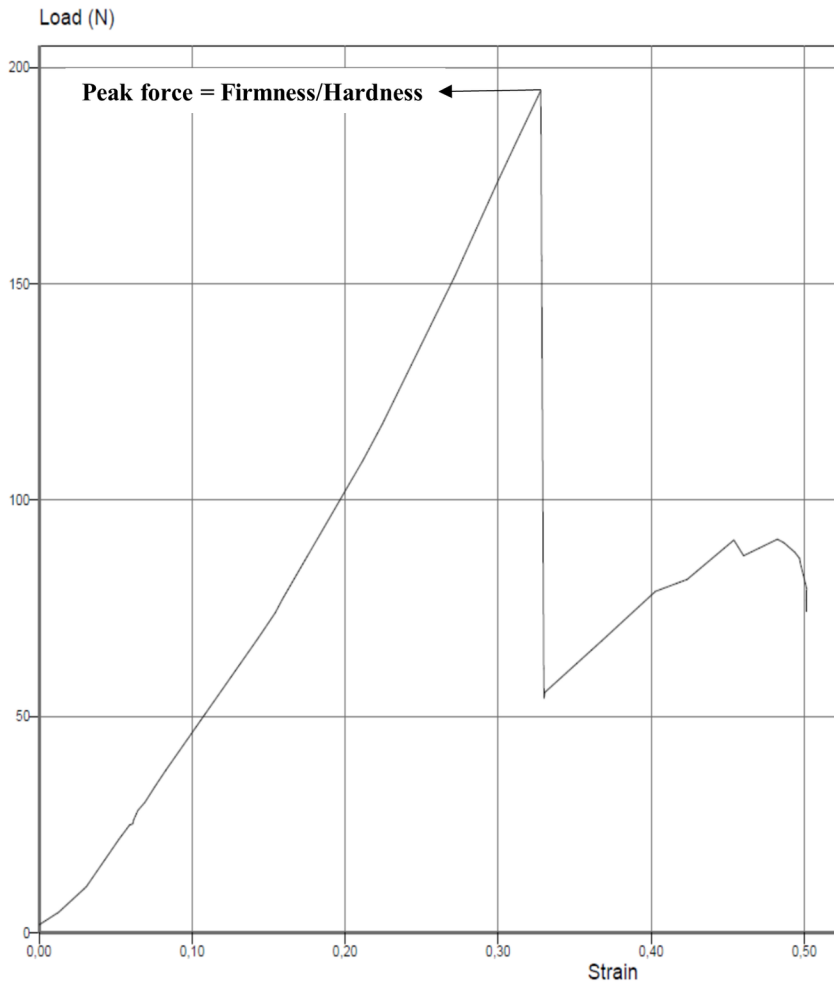
Freeze damage assessment methods for fruits and vegetables	Focused Methods		Global methods				
	Cryo-SEM	CLSM	Texture Analysis		NMR	Drip loss	Colour
			Conventional	Laser-Puff			
Sample preparation	Difficult	Difficult	Easy	Easy	Easy	Easy	Easy
Ability to detect differences between fresh and frozen/thawed sample	×	++++	++++	++++	++++	++++	++++
Ability to distinguish different freezing protocols	++++	++++	++	++	+	++	-
Analysis time (sample preparations + data acquisition and treatment)	+	+	+	+	+++	+	+
Interpretation of measured analytical parameters	Easy	Easy	Easy	Easy	Difficult	Easy	Easy
Nature of sample	F	F/T	F/T	F/T	F & F/T	F/T	F/T
Cost of operation	High	High	Low cost	Low cost	High	Low cost	Low cost
Status of method	OU	NUO	VC	NM	NUO	VC	VC
Error (%)	×	×	Hardness = ± 0.5 YM = ± 3.2	± 0.90	$< \pm 1$	± 0.0016	L = ± 0.02 a = ± 0.21 b = ± 0.15

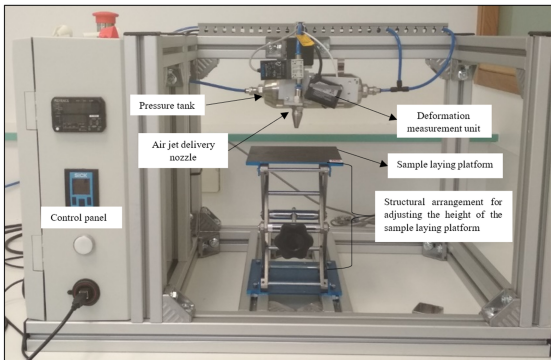
+ = Lowest value; ++++ = Highest value; × = Not applicable; - = No effect.

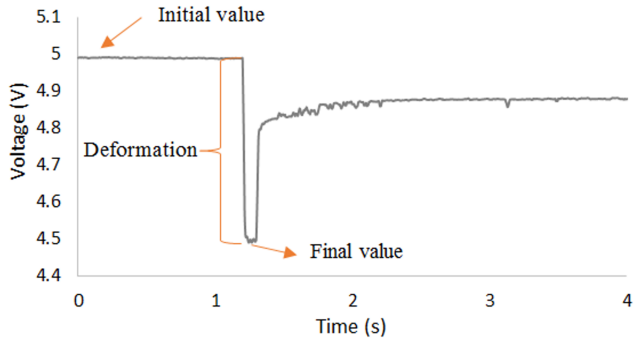
Abbreviations of the words: F = Frozen; F/T = Frozen/Thawed; FD = Freeze dried; OU = Often used; NUO = Not used often; VC = Very common; NM = New method; YM = Young's Modulus.

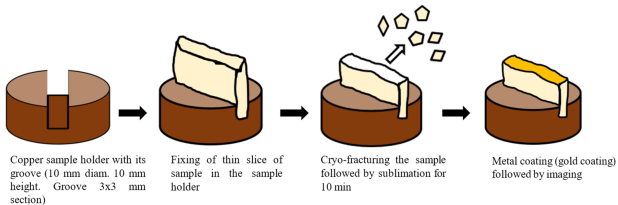
L, a, b are different colour parameters.

907









Sampling

Cylindrical shape (diameter (\emptyset) = 8 mm & height (H) = 5 mm); weight = 0.25 g



Sample was stained in Acridine Orange (0.01%) (pH 7.2) for 2 hours at 4 °C



Freezing under different conditions (at - 18 °C, - 30 °C and - 74 °C)



Thawing of sample at room temperature, followed by slicing using a microtome (80 μ m slice was used for imaging study).



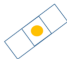
CLSM imaging was then performed using different resolution objective lenses (for e.g. 20X, 10X, 4X, etc.)

(a)

Staining the sample



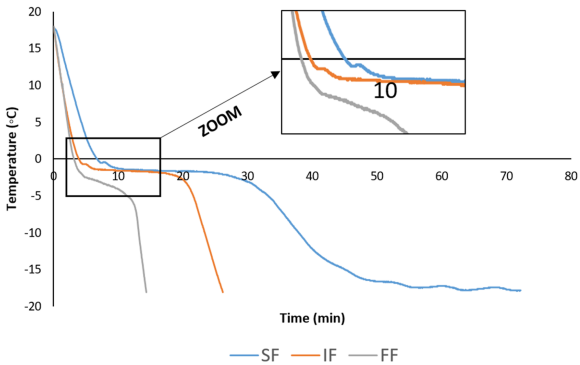
Preparation for imaging

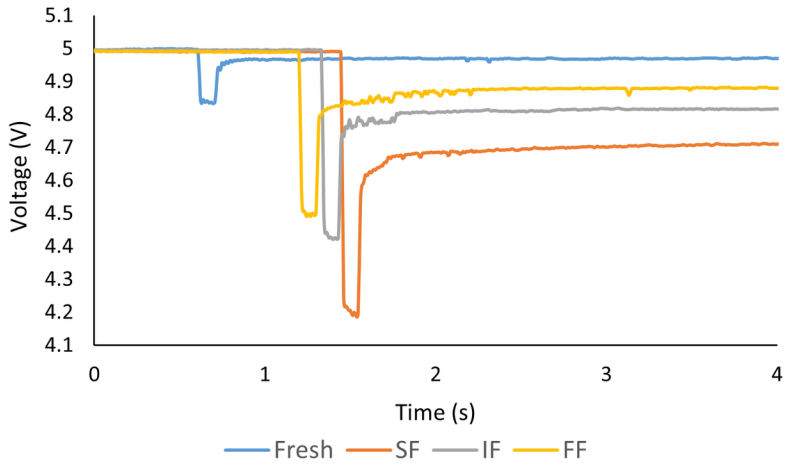


Confocal Laser Scanning Microscope

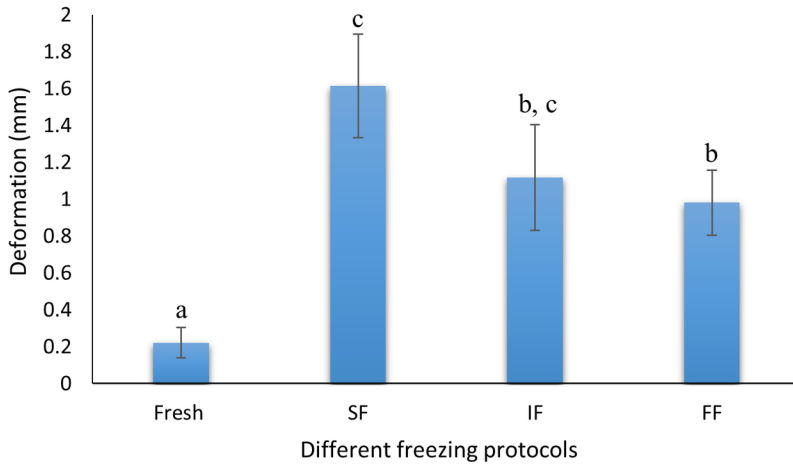


(b)

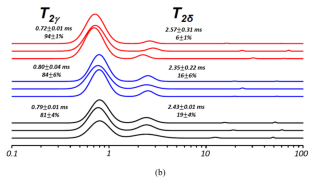
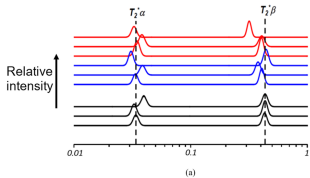




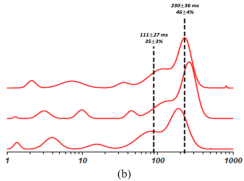
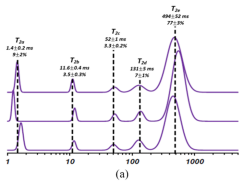
(a)



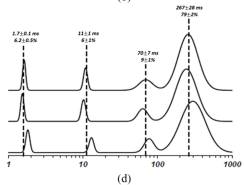
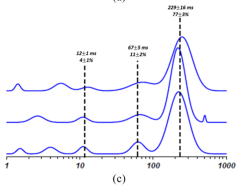
(b)

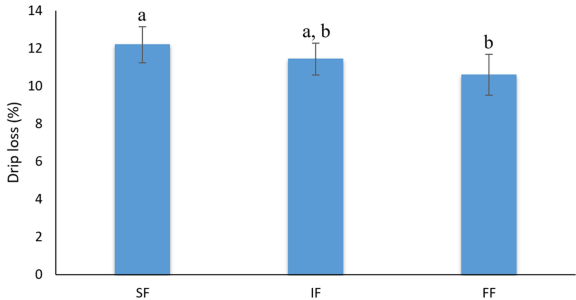


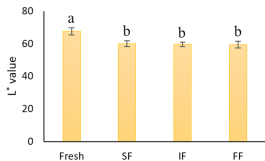
Relative intensity ↑



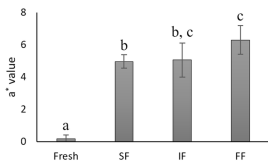
Relative intensity ↑



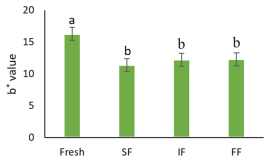




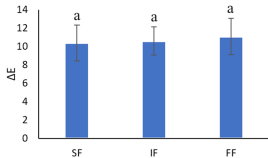
(a)



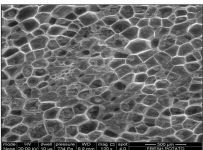
(b)



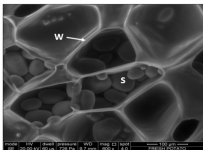
(c)



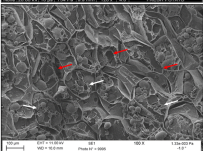
(d)



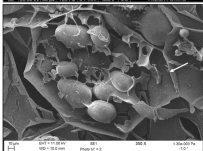
(a)



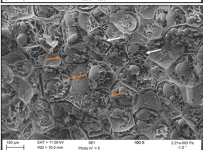
(b)



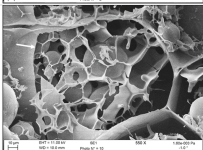
(c)



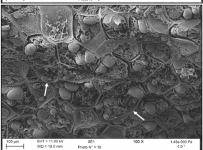
(d)



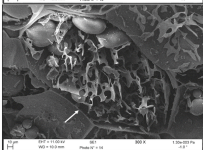
(e)



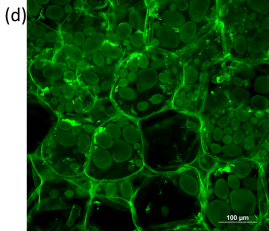
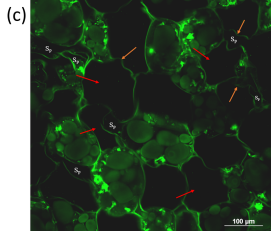
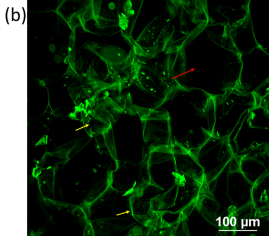
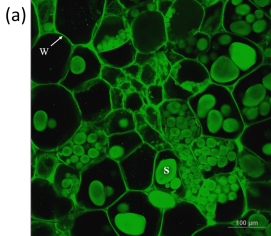
(f)

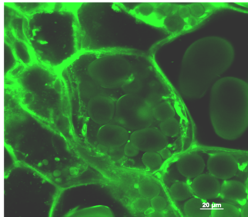


(g)

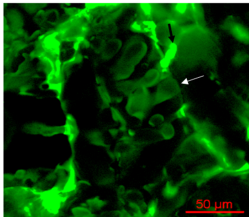


(h)

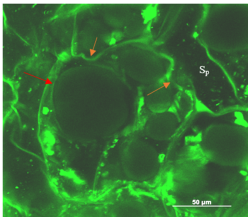




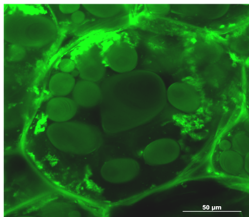
(a)



(b)



(c)



(d)